Pure Appl. Geophys. 170 (2013), 1635–1646

DOI 10.1007/s00024-012-0538-9

Pure and Applied Geophysics

A Probabilistic Tsunami Hazard Study of the Auckland Region, Part II: Inundation Modelling and Hazard Assessment

E. M. Lane,[1] P. A. Gillibrand,[3] X. Wang,[2] and W. Power[2]

Abstract—Regional source tsunamis pose a potentially devastating hazard to communities and infrastructure on the New Zealand coast. But major events are very uncommon. This dichotomy of infrequent but potentially devastating hazards makes realistic assessment of the risk challenging. Here, we describe a method to determine a probabilistic assessment of the tsunami hazard by regional source tsunamis with an "Average Recurrence Interval" of 2,500-years. The method is applied to the east Auckland region of New Zealand. From an assessment of potential regional tsunamigenic events over 100,000 years, the inundation of the Auckland region from the worst 100 events is modelled using a hydrodynamic model and probabilistic inundation depths on a 2,500-year time scale were determined. Tidal effects on the potential inundation were included by coupling the predicted wave heights with the probability density function of tidal heights at the inundation site. Results show that the more exposed northern section of the east coast and outer islands in the Hauraki Gulf face the greatest hazard from regional tsunamis in the Auckland region. Incorporating tidal effects into predictions of inundation reduced the predicted hazard compared to modelling all the tsunamis arriving at high tide giving a more accurate hazard assessment on the specified time scale. This study presents the first probabilistic analysis of dynamic modelling of tsunami inundation for the New Zealand coast and as such provides the most comprehensive assessment of tsunami inundation of the Auckland region from regional source tsunamis available to date.

1. Introduction

Tsunamis represent an infrequent but potentially devastating hazard faced by coastal communities. New Zealand's position on the Pacific "ring of fire" places it at high risk of tsunami inundation. The infrequent nature of tsunami, however, presents a challenge to quantifying the risk posed by them. In some countries the tsunami record is long enough that it can be used to estimate tsunami hazard (Papadopoulos *et al.* 2010; Gonzalez *et al.* 2009; Parsons and Geist, 2008). New Zealand's tsunami record, however, only extends back about 200 years (Downes, 2011), and even then probably does not contain all the tsunamis that occurred in the earlier part of the record due to the sparsely settled coast at the time. Palaeotsunami studies can augment this record, but these records do not give any information as to the source of the event and only traces of the largest events are likely to remain (Goff 2008; Goff *et al.* 2010). As the 2011 Tohoku earthquake and tsunami showed, planners and emergency managers need to be prepared for tsunamis with annual return intervals (ARI) of 1,000 years and longer.

Assessing the full hazard posed by tsunamis to a given region is a difficult task. Sources can be characterised as local, regional and distant. Within these categories there can be different sources too. Although tsunamis generated by earthquakes are the most common, tsunami sources may also include submarine mass failures, volcanic events and even meteorite impacts (Tappin *et al.* 2008; Maeno and Imamura, 2011; Wunnemann *et al.* 2010). Earthquakes of differing sizes, fault geometries and even different slip distributions can produce waves of different magnitudes (Geist, 2002). The wavelength of the tsunami is also a critical factor in determining whether resonances in bays and harbours may amplify the effect of a train of tsunami waves. Probabilistic tsunami hazard assessment (PTHA) provides a framework for comparing the hazard posed by different events and different sources and quantifying areas of higher and lower risk (Geist and

[1] National Institute of Water and Atmospheric Research, 10 Kyle Street, Riccarton, Christchurch, New Zealand. E-mail: Emily.Lane@niwa.co.nz
[2] GNS Science, 1 Fairway Drive, Avalon 5010, PO Box 30-368, Lower Hutt 5040, New Zealand.
[3] *Present Address*: CSIRO Marine and Atmospheric Research, GPO Box 1538, Hobart, TAS 7001, Australia.

Parsons, 2006; Downes and Stirling, 2001). It also allows the hazard posed by tsunamis to be compared with other natural hazards such as earthquakes, floods and storm-tide inundation (Stirling *et al*. 2002).

For more frequent events, distant tsunamis from South America are the biggest tsunami hazard facing New Zealand. Most of the significant tsunamis that have impacted New Zealand in recorded history have been from South America, including the three largest events which occurred in 1868, 1877 and 1960 (Power *et al*. 2007). The most recent event in February 2010 also originated off the Chilean coast. For less frequent events, however, the most potentially devastating tsunami hazard for New Zealand shores arises from local or regional sources. In this study, we examine the tsunami hazard for the Auckland region from regional source tsunamis. The main regional sources are the Tonga-Kermadec and Southern New Hebrides tectonic faults (Power *et al*. 2012). This study takes a probabilistic approach to the hazard. The generation and propagation of a large number of possible tsunamis are modelled, and the predicted inundation from each event is recorded. The probabilistic inundation of the Auckland region on a given time scale can then be assessed, encompassing the uncertainty in the understanding of the geophysical source processes. This study aims to improve knowledge about the probable magnitude of regional tsunami generation mechanisms over a 2,500-year time scale. The 2,500-year ARI is chosen for consistency with similar earthquake hazard studies. The overall objective of the study, therefore, is to determine the probabilistic inundation of the Auckland region's developed areas by regional source tsunamis on a 2,500-year time scale. A companion paper to this one (hereafter referred to as Part I) covers the identification of sources and their characteristics and the creation of a synthetic tsunami record covering 100,000 years. The present paper outlines how the synthetic record can be used to model inundation around Auckland for a range of likely source scenarios and then to determine and map the probable inundation of specific urban areas of the Auckland region for tsunamis at a 2,500-year ARI.

In this paper, we also consider the effects of tides on the predicted inundation resulting from the tsunami strike. Standard practise in tsunami inundation modelling studies is to model inundation at a fixed tidal state, i.e., the variation in tidal height is ignored over the duration of the arrival of the tsunami. In order to develop conservative evacuation plans, modelling is often performed at mean high water springs (MHWS) or an equivalent high water state. However, when the local tidal range is comparable to the height of the tsunami, as is often the case in New Zealand, the tidal state at the time of tsunami arrival can have a significant influence on the subsequent inundation. In a probabilistic analysis, therefore, when many inundation events are considered, the tidal state can have a profound influence on the probabilistic inundation. In this study, we develop a method to include the tidal state at the time of tsunami arrival into the probabilistic analysis. These results are presented in addition to the more conservative approach of modelling the inundation assuming the maximum tsunami wave arrived at MHWS.

2. Methods

Part I showed that tsunamis from the Southern New Hebrides fault do not pose a significant threat to the populated areas of the Auckland coastline. For that reason we focus here on tsunamis from the Kermadec fault. Part I selected the source characteristics for this source based on the 84th percentile of the logic tree branch (the 84th percentile is often used in hazard studies, as it corresponds to the mean plus one standard deviation in a Normal distribution. In this study it corresponded to the Kermadec fault having a maximum magnitude $M_w = 9.2$ and coupling coefficient $C = 0.6$). From this, a synthetic time series of earthquakes spanning a period of 100,000 years was calculated, along with the tsunamis arising from those earthquakes. Using the COMCOT model (Wang and Liu, 2007; Wang *et al*. 2008), they simulated the propagation of these tsunamis to the New Zealand coastline. The largest 100 tsunamis (based on predicted wave height at the coast) were then chosen as the tsunamis to be used within the inundation modelling component of the work. The purpose of the present paper is to describe that inundation modelling, and the methods used to then derive the probabilistic

inundation of selected areas within the Auckland region on a 2,500-year time scale. To that end, in the following sections we describe the inundation model, the preparation of inundation grids, the forcing of the model at the open boundary, and the probabilistic analysis of the inundation results including the incorporation of tidal effects. Some examples of probabilistic inundation for the Auckland region are then presented and discussed.

2.1. The Numerical Model

The numerical model used in this study is a general-purpose hydrodynamics and transport model known as river and coastal ocean model (RiCOM), which solves the standard Reynolds-averaged Navier–Stokes equation (RANS) and the incompressibility condition. It has been tested on a variety of benchmarks against both analytical and experimental data sets (e.g., WALTERS and CASULLI, 1998; WALTERS, 2003, 2005). The model has been previously used to investigate the impact of tsunamis on the New Zealand and other coastline (WALTERS *et al*. 2006a, b, c). In this study the hydrostatic approximation is used, so the equations reduce to the non-linear shallow water equations.

The time intervals that the model solves for are handled by a semi-implicit numerical scheme that avoids stability constraints on wave propagation. The advection scheme is semi-Lagrangian, which is robust, stable, and efficient (STANIFORTH and CÔTÉ, 1991). Wetting and drying of intertidal or flooded areas occurs naturally with this formulation and is a consequence of the finite volume form of the continuity equation and the method of calculating fluxes (flows) through the sides of the triangular elements. At open (sea) boundaries, a radiation condition is enforced so that outgoing waves will not reflect back into the study area, but instead are allowed to realistically continue "through" this artificial boundary and into the open sea. The equations are solved with a conjugate-gradient iterative solver. The details of the numerical approximations that lead to the required robustness and efficiency may be found in WALTERS and CASULLI (1998) and WALTERS (2005).

Bed friction in RiCOM is treated using a quadratic stress law (i.e., stress is proportional to the square of the depth-averaged current velocity). The drag coefficient, C_D, is able to vary spatially. In deep water, C_D has a value of 0.0025, typical of deep sea conditions. In shallow water less than 4 m depth, a power law is applied to enhance the bed stress by up to a factor of four. This recognises the increased frictional stresses acting on flows over very shallow bathymetry and on previously dry land. This approach has been developed over a number of years to improve the performance of the model relative to historical and palaeo-tsunami data.

2.2. The Inundation Grid

RiCOM uses mixed finite element and finite volume methods, and discretizes the RANS equations using unstructured grids of triangular or quadrilateral elements, which permit greater spatial resolution (decreasing element size) in areas of shallow bathymetry or complex coastlines without the need for grid nesting as can be seen in Figs. 1 and 2.

The unstructured grid used in this study is a mesh composed of triangular elements of variable size. The grid has a number of requirements to ensure that model calculations will be accurate and free from excessive numerical errors (HENRY and WALTERS, 1993). The primary requirements are that the triangular elements are roughly equilateral in shape and their grading in size is smooth from areas of high resolution (small elements) in the coastal zone and on land grids to areas of low resolution (large elements) offshore. The grid was generated using the programs GridGen (HENRY and WALTERS, 1993) and TriQGrid (NIWA unpublished software) according to the requirements described above. Layers of elements were generated along the boundaries using a frontal marching algorithm (SADEK, 1980). The size of the triangles was graded as the water depth shoaled. Once a satisfactory computational grid was created and quality assurance test were performed, water depth and land elevation values were interpolated at each node from reference datasets.

The model grid (Fig. 1) covers the region from 170.5E to 177.2E and from 38.2S to 28S on the western edge of the grid and 26.5S on the eastern edge. The spatial resolution of the grid is approximately 2 km in deep water at the outer edge of the

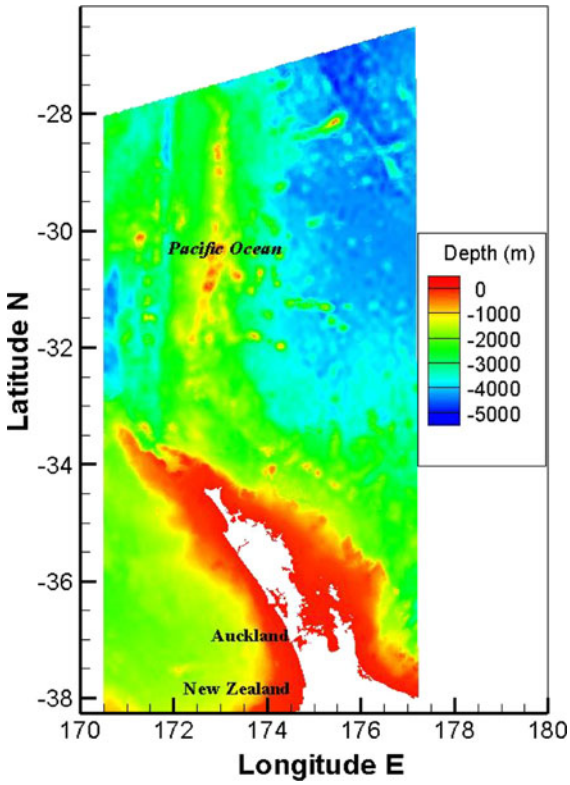

Figure 1
The Auckland region tsunami inundation model grid. The grid is made up of *triangular* elements. Water depth (m) at each element relative to mean sea level is indicated by the *colouring*. The size of the elements ranges from 5 to 10 m in the inshore areas where inundation is predicted to 2 km in the outer reaches of the grid

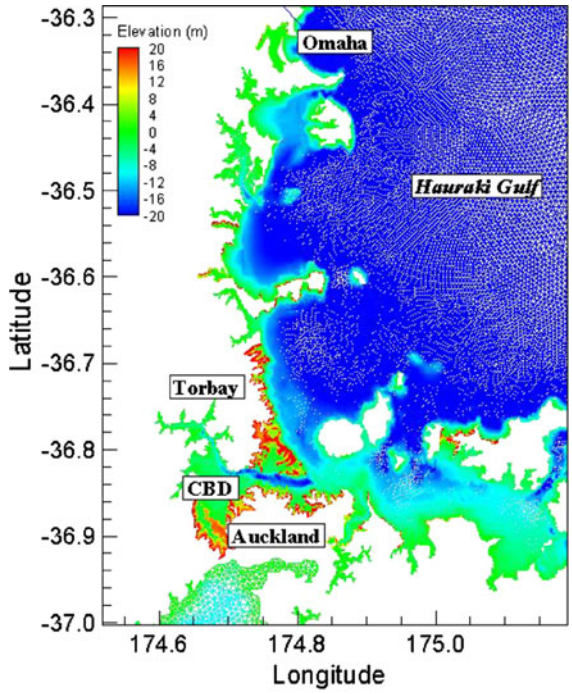

Figure 2
Magnified view of the model grid around Auckland. Individual triangular grid elements are *coloured* according to the elevation (m) of the seabed or land surface relative to mean sea level. The *triangular* elements reduce in size towards the coastline, evidenced by the *solidifying* of the *colouring*

grid, grading into several hundred metres in the shallow coastal areas, and then to 5–10 m in the areas where inundation modelling is to be predicted. Model bathymetry was interpolated from a combination of ETOPO1 for the deep water, blending into NIWA regional and coastal data sets in the shallower coastal waters around New Zealand.

Inundation is modelled by creating a grid of land topography and merging it into the bathymetric grid, providing a seamless transition from ocean onto land. The topography of the land grids is derived from light detection and ranging (LiDAR) data; for the present study, LiDAR data were provided by Auckland Regional Council. Raw LiDAR data typically have a spatial resolution of 2 m and a vertical accuracy of about 10 cm. For the model grid, the bare earth LiDAR topography data are gridded into a DEM with a spatial resolution of 10 m. A magnified view of the model grid focussing on these land grids is shown in Fig. 2. The high spatial resolution of the land grids generates a high computational demand and imposes a limit on the extent of land over which inundation can be modelled in any one simulation; thus, rather than modelling the entire coastal zone, several land grids, each covering a small area in particular locations, are built and merged into the bathymetric grid. Thus, a series of areas were chosen for inundation modelling due to their perceived risk (i.e., either more exposed to tsunami hazard or higher population areas). Figure 3 shows the areas where inundation modelling was simulated. In this paper, results are presented for the northern most of the areas, Omaha, which is shown as area one in Fig. 3.

2.3. Initial Conditions and Boundary Forcing

The inundation simulations began at rest, with a uniform sea surface height, either MHWS or highest

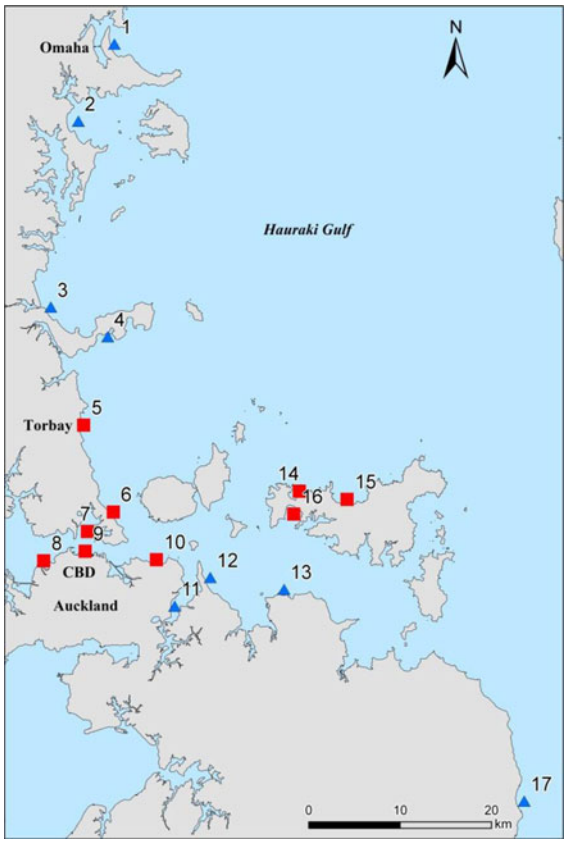

Figure 3
Areas where probabilistic inundation modelling was undertaken. Area 1 is Omaha where results are given for in Sect. 3. Section 4 also mentions Torbay (area 5) and the Central Business District (CBD, area 9)

astronomical tide (HAT), specified throughout the domain. The model was forced by the time histories of water level and current velocity extracted from the COMCOT simulations of tsunami propagation (Part I) at the locations of grid nodes along the eastern edge of the RiCOM model domain (Fig. 1). The incident wave conditions (water height and normal velocity) were specified in RiCOM using a radiating boundary condition (FLATHER, 1976; MARCHESIELLO *et al*. 2001), allowing reflections from the coast of New Zealand to pass out through the eastern boundary without distorting the incident wave signal. Radiating boundary conditions were also applied along the northern, western and southern boundaries of the RiCOM grid, allowing the propagating wave to pass through without sending spurious reflections back into the model domain. Although there is the potential for amplitude suppression of the wave near the unforced boundaries this is minimised because the edge of the domain is parallel to the wave front. Furthermore, the area of interest is far from the unforced boundaries and experiments with larger domains showed that the results were not affected by only forcing one side of the domain. Comparisons with the forcing model within the domain showed reasonable levels of agreement.

2.4. *Probabilistic Analysis of Inundation*

The 100 tsunami inundation simulations were used to calculate the annual exceedance probabilities (AEP) of tsunami inundation as discussed below. In addition, AEP can also be calculated for other quantities, such as maximum speed. Also discussed below is a methodology for also incorporating tidal state at the tsunami arrival time into the calculations. This differs from previous methods (MOFJELD *et al*. 2007) in that actual time series from the inundation modelling and tidal cycles is used in the analysis. Because tidal and tsunami current speeds are considerably more spatially variable than water levels, this new technique does not work for maximum speed calculations.

2.4.1 *Monte Carlo Simulation of AEP Excluding Tides*

Calculation of the tsunami inundation AEP for different levels is performed using a Monte Carlo method. Part I describes the method for identifying N scenarios which represent a Monte Carlo simulation of all (or at least the biggest) tsunamis impacting the region within an L year period (where L is sufficiently large). For each of these scenarios, inundation modelling is undertaken. This provides inundation depths at each point, x, viz. $I_i(x), \quad i = 1, \ldots, N$. The probability that a given point x_0 will be inundated to greater than depth h_0 within a given year is then:

$$P\left(\max_{\text{annual}}(I(x_0)) > h_0\right) = \frac{1}{L}\sum_{i=1}^{N}[I_i(x_0) > h_0]$$
$$\text{where } [f] = \begin{cases} 1 & \text{if } f \text{ is true} \\ 0 & \text{if } f \text{ is false} \end{cases}. \qquad (1)$$

So, for the 1:L_0 year exceedance of h_0 inundation area (i.e., the area which is expected to be inundated by a tsunami to a depth of h_0 at least once every L_0 years), it remains to find

$$\left\{x : P\left(\max_{\text{annual}}(I(x)) > h_0\right) \geq \frac{1}{L_0}\right\}. \qquad (2)$$

In the case modelled here, this is a representative sample of the one hundred tsunamis with largest impact on the east coast of the Auckland region over 100,000 years. Thus, $N = 100$ and $L = 100{,}000$. In order to find inundation exceedances for 2,500-year ARI the number of times inundation exceeds a set level, h_0, is summed up for each point. If this is greater than $L/L_0 = 100{,}000/2{,}500 = 40$, then that point is expected to inundate to that level at least once, on average, every 2,500 years. Inundation exceedances for $h_0 = 0.1$, 0.5, 1.0, 1.5, 2 and 2.5 m were calculated.

These inundation scenarios were calculated with the assumption that the maximum wave height arrived at MHWS as a simple way of incorporating the tides into the calculations. In the case of moderate-amplitude tsunami, the point in the tidal cycle where the tsunami arrives can have a significant effect on the actual sea level that occurs and hence the actual inundation that results. Below a method to incorporate tidal effects into the calculations is outlined.

2.4.2 *Monte Carlo Tsunami Simulations Including Tides*

Give sufficient computing power, tides could be added into the Monte Carlo simulations by brute force (i.e., by randomly selecting not only the event but also the tidal state when it occurs, and modelling both tsunamis and tides together). This approach would, however, significantly increase the number of inundation simulations required in order to get a representative sample.

Methods to include the tides within probabilistic tsunami inundation assessments are still being developed internationally (e.g., Gonzalez *et al*. 2009). The current state-of-the-art is to model a representative maximum wave height, assume that the maximum arrival has a period of 20 min and that its height falls off exponentially with time. This information can then be used in conjunction with tidal information to sample the probability density function (PDF) of possible inundation depths (Gonzalez *et al*. 2009; Mofjeld *et al*. 2007). However, this approach does not include full inundation modelling. By modelling inundation explicitly, extra information about wave arrivals in each area is obtained.

The method outlined in this paper uses the time series of water level at each inundation area due to the tsunami together with local tidal information for that area to develop a PDF of maximum sea level. Lower frequency fluctuations in storm surge and MLoS (monthly to annual variations in the mean level of the sea) are not included in this analysis, but could also further affect the PDF. Because the storm surge and the MLoS occur on sufficiently slow timescales that they do not vary significantly over the tsunami event, these could be taken into account by convolving the maximum sea level PDF with storm surge and MLoS PDF. This is beyond the scope of the present study, however.

In order to incorporate tidal effects, the tsunami inundation is re-modelled with the baseline set at HAT rather than MHWS. From this modelling, the inundation is determined from the highest possible water level due to tide and tsunami, rather than that from a tsunami arriving at an "average" high tide. The PDF, g_i, derived from the tsunami time series (scenario i) and the local tidal series is then used to weight successively reduced levels of inundation until an element is dry. In addition to this, any wet element which becomes disconnected from the sea as the inundation depths are ramped back has its inundation set to zero, on the assumption that the threshold level needed to inundate this area has not been reached. Again, the inundation over a given threshold h_0 from all the scenarios is summed and those elements whose contribution sum to more than 40 are marked as being inundated by an h_0-level at least once, on average, every 2,500 years. The difference from the previous (non-tidal) approach is that, within each scenario, there are different contributions weighted by the PDF.

The probability that a given point x_0 will be inundated to greater than depth h_0 within a given year is then:

$$P\left(\max_{\text{annual}}(I(x_0)) > h_0\right) = \frac{1}{L}\sum_{i=1}^{N}\sum_{j=1}^{M} g_{ij}\mathrm{d}\eta\left[I_{ij}(x_0) > h_0\right]$$

$$= \frac{1}{L}\sum_{i=1}^{N}\sum_{j=1}^{M} g_{ij}\mathrm{d}\eta[I_i(x_0) > h_0 + (M-j)\mathrm{d}\eta]. \quad (3)$$

where g_{ij} is the probability density of an element being inundated during tsunami event i for bin j (as calculated above from the tidal and tsunami time series), M is the number of bins in the PDF and $\mathrm{d}\eta$ is the bin size.

Thus the 1:L_0 year exceedance of h_0 inundation area is calculated as before,

$$\left\{x : P\left(\max_{\text{annual}}(I(x)) > h_0\right) \geq \frac{1}{L_0}\right\}. \quad (4)$$

Tsunami and tidal time series were collected for each of the areas where inundation modelling was performed (Fig. 3). Tsunami time series were stored during the modelling process. Tidal time series for different regions were determined using a range of co-tidal charts, sea level gauge analysis and a tidal harmonic model (R. BELL, personnel communication, based on data from Ports of Auckland Ltd.; results from harmonic model Tide2D, WALTERS *et al*. 2001; WALTERS, 2005).

3. Results

3.1. Variations of Maximum Water Elevation with Tidal State

The variation of the maximum water level with the tidal state at the tsunami arrival time depends upon the details of the tsunami time series. To illustrate this, Fig. 4 shows two tsunami time series (a) and (b) for location 1 in Fig. 3. By combining each time series with the local tidal time series at different temporal offsets, the different possible maximum sea levels and the probability that they will occur can be calculated. Figure 4c, d show this for the two time series. Where there is one large arrival considerably bigger than the rest of the waves (Fig. 4a), the PDF is very similar to the tidal PDF plus the maximum wave height (Fig. 4c). For more complex wave arrivals (Fig. 4b), the PDF is similarly more complex (Fig. 4d). Figure 5 shows the time series of the 'same' tsunami arriving at different times (offsets) in a typical tidal cycle, and illustrates how the maximum sea level achieved depends on the time of tsunami arrival relative to the tidal cycle. For example in the case shown, peak water levels occur when the tsunami arrival is offset by about 20 h and the maximum wave arrival coincides with high tide. With an offset of about 13 h, the maximum wave arrives at low tide and its impact on water level is effectively cancelled.

3.2. Probabilistic Regional Wave Heights for Auckland

The 2,500-year probabilistic exceedance levels for wave height (relative to mean sea level) for the region east of Auckland from regional tsunamis are shown in Fig. 6. As can be readily seen, the east coast of Great Barrier Island (in the top right hand corner of the figure) bears the brunt of the inundation with probabilistic wave heights of up to 10 m. The upper east coast is also reasonably exposed to regional tsunami. There do not appear to be any significant resonances initiated by the tsunamis in the upper harbour areas. Further up the harbour and in areas sheltered by islands the tsunami hazard appears to be fairly low.

3.3. Probabilistic Tsunami Hazard Assessment

Probabilistic inundation at the 2,500-year ARI for depths of 0.1, 0.5, 1, 1.5, 2 and 2.5 m are shown in Fig. 7. These should be understood as illustrating the area predicted to be inundated to at least that depth at least once every 2,500 years, on average, over a long (e.g., 100,000 years) period of time. Two versions of the map are shown: the first version shows predicted inundation if all tsunamis occur at MHWS; the second version shows predicted inundation if variation in tidal height is taken into account during the probabilistic calculations. Because this is a probabilistic study, there is no one particular tsunami event that necessarily inundates to this level everywhere in the model domain. The maps represent an amalgamation of the results from the 100 model tsunami simulations performed. As well as the probabilistic inundation, probabilistic maximum speed maps were

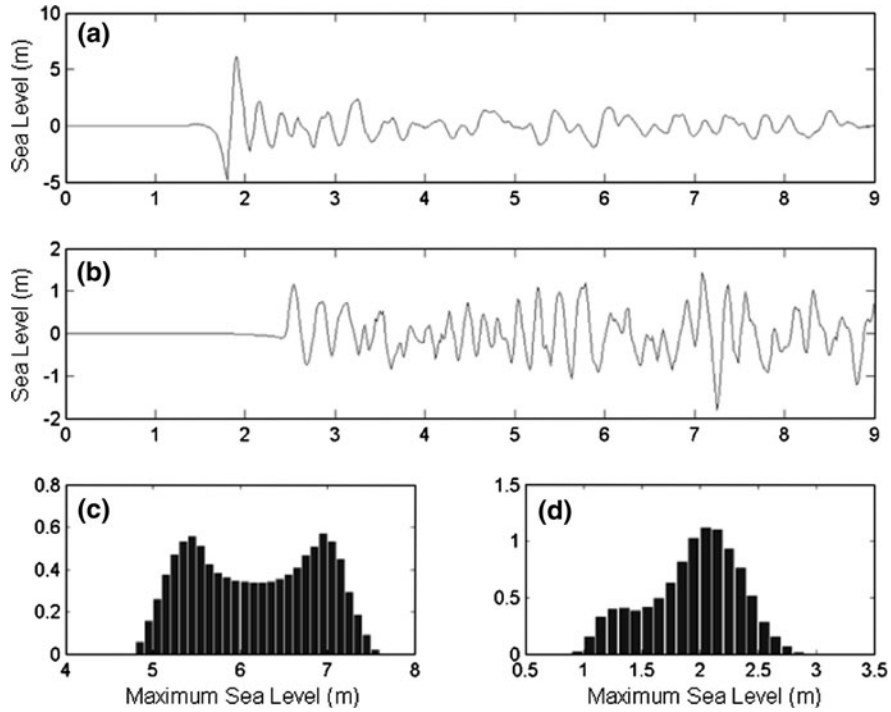

Figure 4
Time series of the largest (**a**) and smallest (**b**) tsunamis arriving at location 1 (see Fig. 3) and the PDFs of the maximum sea level attained given that the tsunami could arrive at any point in the tidal cycle (**c**, **d**, respectively)

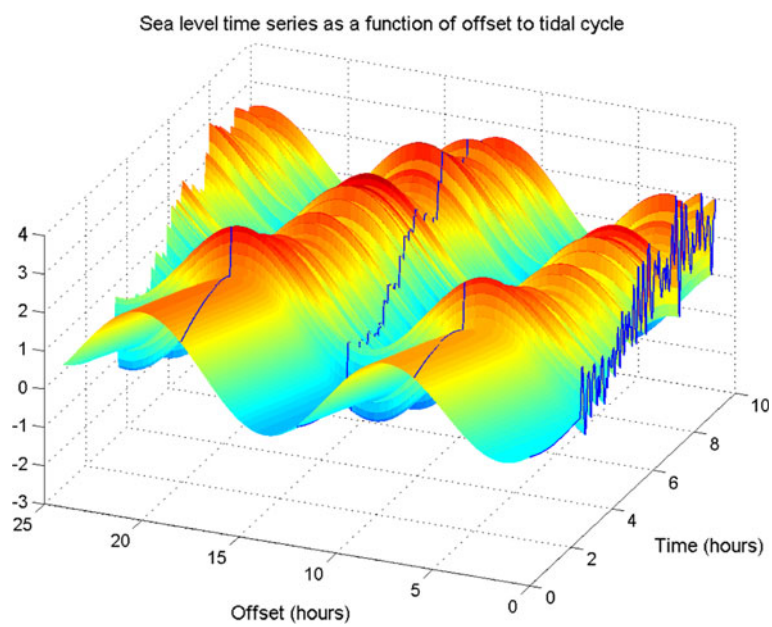

Figure 5
Time series of sea level heights during a tsunami as a function of time (h) and offset against a 12-h tidal cycle. The *blue lines* represent time series with 0, 6, 12 and 18 h offset

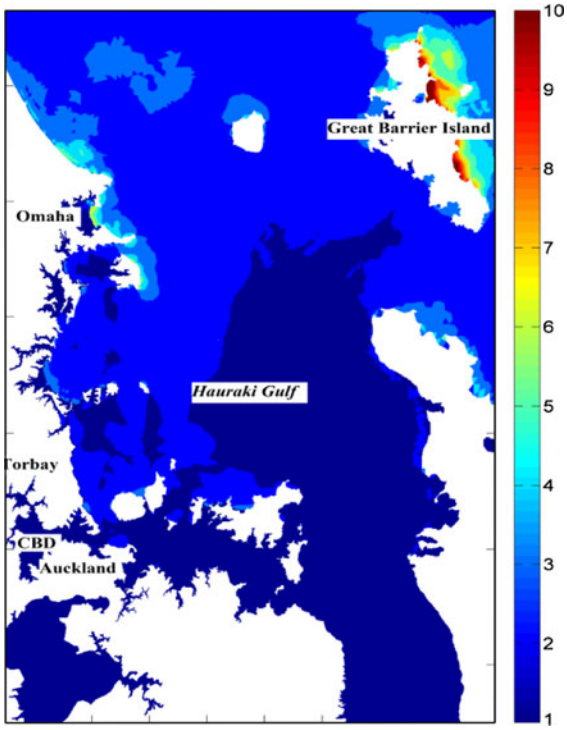

Figure 6
2,500-year ARI exceedance levels for water level (metres above mean sea level) due to regional tsunamis for the Auckland region

also calculated (although not shown here). Again, these represent an amalgamation of the results from the 100 model tsunami simulations, but do not include tidal effects.

It is evident that including the tidal effects reduces the inundation depth and extent compared to the situation at MHWS. This result was also apparent for the other modelled locations around Auckland. Given that the majority of tidal heights are below MHWS this is not necessarily a surprising result; however, it is useful to be able to quantify these differences.

4. Discussion

The low likelihood but potentially devastating results of major tsunami impacts makes careful assessment of the risk essential. Local planning authorities should not overspend resources on planning for an event that is very unlikely on infrastructure planning time scales. Nevertheless, it is incumbent on them to be fully prepared for events with a reasonable probability of occurring on those time scales. The best hazard assessment possible is therefore invaluable. Previously, tsunami inundation modelling generally used a fairly high baseline sea level such as MHWS in order to provide conservative, "worst case" estimates of inundation. Although potentially justified on safety grounds, this approach makes it difficult to compare different hazards when trying to apportion scant resources on mitigation measures.

By developing a method to incorporate tidal influence into the predicted inundation, we have provided a more realistic probabilistic hazard assessment for Auckland on a 2,500-year time scale from regional tsunamis. Apart from the very largest potential tsunamis, the tidal range around the New Zealand coast is of comparable magnitude to the tsunami wave heights. Should a moderate tsunami strike at low tide the hazard is effectively nullified. Accounting for tides in macro- or meso-tidal regions better balances the hazard assessment between actual risk and cost implications. Moreover, the approach we have presented here avoids the excessive computational demands that would be required by modelling all tsunami scenarios at a range of tidal states, and can be adopted using inundation predictions with any tsunami model provided that local tidal height information are known.

It should be noted that the method used here to account for the influence of tidal state on coastal inundation by tsunamis does not include dynamic interactions between the tide and the tsunami. Modelling by KOWALIK and PROSHUTINSKY (2010) of the Cook Inlet showed that for strong tidal signals (e.g., tidal range of 8 m in that case) there were interactions between the tides and the tsunami. For instance, the total water depth is modified by the tidal state during the passage of the wave, as are current speeds and, hence, bed friction. These effects may modify the propagation and subsequent inundation caused by the tsunami. In order to include these nonlinear interactions, full hydrodynamic modelling of tsunami inundation at all tidal states would be required. This would significantly increase the computational load as spin up of the tidal state would be required in addition to the tsunami modelling. As the tidal range is much smaller in the Auckland region we expect

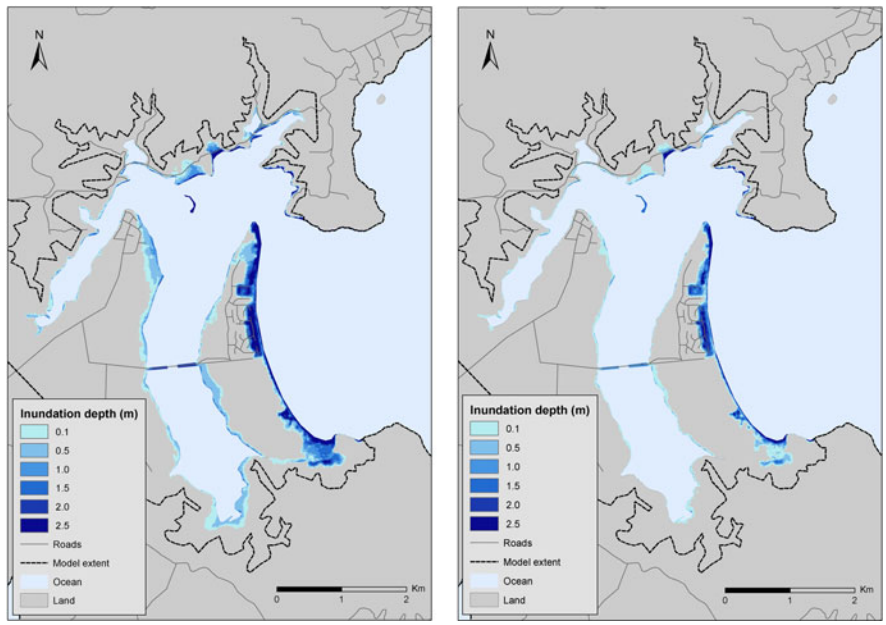

Figure 7
2,500-year ARI exceedances for regional probabilistic tsunami inundation for Omaha at MHWS (*left*) and including tidal effects (*right*)

these effects to be relatively minor. Furthermore, by modelling the tsunami at HAT, we are taking a more conservative approach and are more likely to overestimate the inundation at lower tidal levels than the reverse.

This assessment only includes regional tsunamis. Bayesian means (GREZIO *et al*. 2010) or joint probability methods (GONZALEZ *et al*. 2009) could be used to link the probabilities from this assessment with the hazard due to far-field tsunamis and local and regional tsunamis due to other sources.

4.1. Effects of Limiting Number of Tsunami Modelled

The PTHA including tidal effects only uses the top 100 tsunamis out of approximately 3,000 possible tsunamigenic earthquakes that were modelled for the 100,000 year time frame of the Monte Carlo simulations. Thus, it is possible that smaller tsunamis combined with a higher tide could cause greater inundation than a moderate event at low tide. If the tsunami was smaller than the top 100 its impact would not be included in this assessment. To investigate the possible effects of this, the smallest of the 100 tsunamis modelled with the 2,500 AEP level are compared.

First a cumulative plot of all the possible combinations of tsunami wave height (from the 100 largest events) and the varying tidal heights for each point is created. The highest expected sea level in 2,500-years (i.e., that sea level that occurs 40 times in 100,000 years) is identified. The proportion of the PDF for the smallest tsunami arrival (smallest tsunami PDF) that is larger than this critical value is then calculated. The percentage of the smallest tsunami PDF that lies above the expected 2,500-year level provides an indication of the importance of the tidal contribution to inundation at that location; a larger percentage means that a small tsunami may have a significant influence on the probabilistic inundation in the event that it arrives at or around high spring tide.

Table 1 demonstrates this point: the percentage of the smallest tsunami PDF above the 2,500-year AEP inundation level is presented together with data on tidal heights and tsunami waves heights at each location. Results are given for three areas (A, B and C) which correspond to Omaha, Torbay and CBD (numbers 1, 5 and 9, respectively, in Fig. 3). In area A (where the inundation modelling is shown) the HAT is relatively low and the tsunami heights are large, all subsequent tsunamis modelled will be smaller than the 2,500 year return period tsunami

Table 1

Highest and lowest high tides and highest and lowest maximum tsunami wave heights for selected points

Area	HAT (m)	Lowest high tide (m)	Maximum tsunami wave height (m)	Minimum tsunami wave height (m)	2,500-year height (m)	Percentage smallest tsunami above
A	1.4	0.5	6.2	1.4	4.8	0
B	1.6	0.7	1.8	0.7	1.9	12
C	1.8	0.8	0.9	0.3	1.5	21

and thus will not contribute to the analysis. In area B the tsunami heights are not as large and there is some overlap between the smallest tsunami PDF and the 2,500 year AEP height. In this case Monte Carlo modelling with additional events may slightly change the 2,500 year AEP. In area C, the overlap exceeds 20 %. In this location, the HAT is relatively large compared to the other locations, and the height of the tsunami small. The state of the tide at the time of tsunami arrival, therefore, has a greater influence on the extent of the inundation. Smaller tsunamis than were modelled in this study may influence the probabilistic inundation. In this case it would be prudent to include more scenarios in the Monte Carlo simulation or to use the modelling at MHWS.

5. Summary and Conclusions

This study presents the first probabilistic analysis of dynamic modelling of tsunami inundation for the New Zealand coast. In all, inundation of the Auckland region from 100 tsunami events has been dynamically modelled, and the results synthesized into probabilistic maps of inundation depth and maximum current speed for tsunamis with 2,500-year ARI. The simulations conducted assuming tsunami arrival coincides with mean high water spring tides provide conservative estimates of probabilistic inundation suitable for emergency management and planning. Incorporating varying tidal states provides more accurate estimates of the probabilistic inundation, but the results for the present study were hindered at some locations because the influence of smaller tsunamis on the probabilistic inundation at some locations was not captured. The study provides the most comprehensive assessment of tsunami inundation of the Auckland region from regional source tsunamis available to date.

Acknowledgments

Tide gauge data were provided by Ports of Auckland Ltd. We thank Jade Arnold and Jen Dumas for preparing the inundation grids of the Auckland region. Julian Sykes prepared Fig. 7. We thank Greg Holland and Rob Bell for their support during the project planning and delivery, and Roy Walters for his continued collaboration with the RiCOM model. This study was funded by Auckland Regional Council.

References

Downes, G. L., and Stirling, M. W. (2001). *Groundwork for development of a probabilistic tsunami hazard model for New Zealand*, ITS 2001 Proceedings, session 1, number 1–6.

Downes, G. L. (2011). *New Zealand Tsunami Database,* (unpublished).

Flather, R. A., 1976. *A tidal model of the northwest European continental shelf*, Memoires de la Societe Royale des Sciences de Liege, *6* (10), 141–164.

Geist, E. L., and Parsons, T. (2006). *Probabilistic analysis of tsunami hazards*, Natural Hazards *37*(3), 277–314.

Geist, E. L. (2002). *Complex earthquake rupture and local tsunami*. J. Geophys. Res. *107,* B5, doi:10.1029/2000JB000139.

Goff, J. R. (2008). *The New Zealand palaeotsunami database*, NIWA technical report 131.

Goff, J., Pearce, S., Nichol, S. L., Chagué-Goff, C., Horrocks, M., and Strotz, L. (2010), *Multi-proxy records of regionally-sources tsunamis, New Zealand,* Geomorphology, *118*, 369–382.

Gonzalez, F. I., Geist, E. L., Jaffe, B., Kanoglu, U., Mofjeld, H., Synolakis, C. E., Titov V. V., Arcas D., Bellomo D., Carlton D., Horning, T., Johnson, J., Newman, J., Parsons, T., Peters, R., Peterson, C., Priest, G., Venturato, A., Weber, J., Wong, F., and Yalciner, A., (2009). *Probabilistic tsunami hazard assessment at Seaside, Oregon, for near- and far-field seismic sources,* J. Geophys. Res. *114*., C11023, doi:10.1029/2008JC005132.

GREZIO, A., MARZOCCHI, W., SANDRI, L., and GASPARINI, P. (2010). *A Bayesian procedure for Probabilistic Tsunami Hazard Assessment,* Nat. Hazards *53*(1), 159–174.

HENRY, R. F. and WALTERS, R. A. (1993). *A geometrically-based, automatic generator for irregular triangular networks,* Commun. Numer. Meth. En., *9*, 555–566.

KOWALIK, Z. and PROSHUTINSKY, A. (2010). *Tsunami-tide interactions: A Cook Inlet case study,* Cont. Shelf Res. *30*(6), 633–642.

MAENO, F. and IMAMURA, F. (2011). *Tsunami generation by a rapid entrance of pyroclastic flow into the sea during the 1883 Krakatau eruption, Indonesia.* J. Geophys. Res. *116*.

MARCHESIELLO, P., MCWILLIAMS, J. C., SHCHEPETKIN, A. (2001) *Open Boundary conditions for long-term integration of regional oceanic models.* Ocean Model. *3*, 2–20.

MOFJELD, H. O., GONZALEZ, F. I., TITOV, V. V., VENTURATO, A. J., and NEWMAN, J. C. (2007). *Effects of tides on maximum tsunami wave heights: Probability distributions*, J. Atmos. Oceanic Tech. *24*(1), 117–123.

PAPADOPOULOS, G.A., DASKALAKI, E., FOKAEFS, A., and GIRALEAS, N. (2010). *Tsunami hazard in the eastern Mediterranean Sea: Strong Earthquakes and tsunamis in the West Hellenic Arc and trench system,* J. Earthquake Tsunami *4*(3), 145–179.

PARSONS, T. and GEIST, E. L. (2008), *Tsunami Probability in the Caribbean Region,* Pure Appl. Geophys. *165*(11–12), 2089–2116.

POWER, W., DOWNES, G., and STIRLING, M. (2007) *Estimation of Tsunami Hazard in New Zealand due to South American Earthquakes,* Pure Appl. Geophys., *164*, 547–564.

POWER, W. L., WANG, X., WALLACE, L., and REYNERS, M. (2012). *Tsunami hazard posed to New Zealand by the Kermadec and Southern New Hebrides Subduction Margins: An Assessment Based on Plate Boundary Kinematics*, Pure Appl. Geophys., *169,* 1–36.

SADEK, E. A. (1980). *A scheme for the automatic generation of triangular finite elements*, Int. J. Num. Meth. Eng. *15*, 1813–1822.

STANIFORTH, A. and CÔTÉ, J. (1991). *Semi-Lagrangian integration schemes for atmospheric models - a review*, Mon. Weather Rev. *119*, 2206–2223.

STIRLING, M. W., MCVERRY, G. H., and BERRYMAN, K. R. (2002). *A new seismic hazard model for New Zealand*, Bull. Seismol. Soc. Am. *92*(5),1878–1903.

TAPPIN, D. R., WATTS, P., and GRILLI, S. T. (2008). *The Papua New Guinea tsunami of 17 July 1998: anatomy of a catastrophic event,* Nat. Hazards Earth Sys. Sci. *8*(2), 243–266.

WALTERS, R. A., and CASULLI, V. (1998). *A robust, finite element model for hydrostatic surface water flows.* Comm. Numer. Meth. En. *14*, 931–940.

WALTERS, R. A., GORING, D. G., and BELL, R. G. (2001). *Ocean tides around New Zealand,*. New Zeal. J. Marine Freshwater Res. *35*(3), 567–579.

WALTERS R. A. (2003) *Tsunami runup: model development and testing*. In *Long waves symposium, AUTh, Thessaloniki, Greece*, (eds. Briggs M, Koutitas C.) 25–27 Aug 2003. pp 289–296.

WALTERS, R. A. (2005). *A semi-implicit finite element model for non-hydrostatic (dispersive) surface waves,* Int. J. Num. Meth. Fluid *49*, 721–737.

WALTERS, R. A., BARNES, P., and GOFF, J. (2006a). *Locally generated tsunami along the Kaikoura coastal margin: Part 1. Fault ruptures*. New Zeal. J. Marine Freshwater Res. *40*(1): 1–17.

WALTERS, R. A., BARNES, P., LEWIS, K., GOFF, J., and FLEMING, J (2006b). *Locally generated tsunami along the Kaikoura coastal margin: Part 2. Submarine landslides,* New Zeal. J. Marine Freshwater Res. *40*(1), 18–34.

WALTERS, R. A., GOFF, J., and WANG, K. (2006c). *Tsunamigenic sources in the Bay of Plenty, New Zealand.* Sci. Tsunami Haz. *24*, 339–357.

WANG, X. and LIU, P. L.-F. (2007). *Numerical simulations of the 2004 Indian ocean tsunami - coastal effects*. J. Earthquake Tsunami *1*(3), 273–297.

WANG, X., ORFILA, A. and LIU, P. L.-F. (2008). *Numerical simulations of tsunami runup onto a three-dimensional beach with shallow water equations*. In *Advanced numerical models for simulating tsunami waves and runup*. (eds. LIU, P.L.-F.; YEH, H.H; SYNOLAKIS, C.) (Hackensack, NJ: *World Scientific. Advances in coastal and ocean engineering* 10.) p. 249–253.

WUNNEMANN, K., COLLINS, G. S., and WEISS, R. (2010*). Impact of a cosmic body into earth's ocean and the generation of large tsunami waves: insight from numerical modeling*. Rev. Geophys. *48.*

(Received February 2, 2012, revised June 12, 2012, accepted June 18, 2012, Published online August 10, 2012)